MEDICAL ROBOTS

Using robotics to move a neurosurgeon's hands to the tip of their endoscope

Karl Price[1]†, Joseph Peine[1]‡, Margherita Mencattelli[1], Yash Chitalia[1]§, David Pu[1]¶, Thomas Looi[2], Scellig Stone[3], James Drake[2], Pierre E. Dupont[1]*

A major advantage of surgical robots is that they can reduce the invasiveness of a procedure by enabling the clinician to manipulate tools as they would in open surgery but through small incisions in the body. Neurosurgery has yet to benefit from this advantage. Although clinical robots are available for the least invasive neurosurgical procedures, such as guiding electrode insertion, the most invasive brain surgeries, such as tumor resection, are still performed as open manual procedures. To investigate whether robotics could reduce the invasiveness of major brain surgeries while still providing the manipulation capabilities of open surgery, we created a two-armed joystick-controlled endoscopic robot. To evaluate the efficacy of this robot, we developed a set of neurosurgical skill tasks patterned after the steps of brain tumor resection. We also created a patient-derived brain model for pineal tumors, which are located in the center of the brain and are normally removed by open surgery. In comparison, testing with existing manual endoscopic instrumentation, we found that the robot provided access to a much larger working volume at the trocar tip and enabled bimanual tasks without compression of brain tissue adjacent to the trocar. Furthermore, many tasks could be completed faster with the robot. These results suggest that robotics has the potential to substantially reduce the invasiveness of brain surgery by enabling certain procedures currently performed as open surgery to be converted to endoscopic interventions.

INTRODUCTION

More than 380,000 intracranial neurosurgical procedures are performed annually in the United States to treat brain tumors, trauma, epilepsy, hydrocephalus, and vascular lesions (*1*). Most intracranial operations are performed as open microsurgery, which involves removing a portion of the skull and using handheld instruments while visualizing the brain through a microscope (Fig. 1, A and B). If the surgical site is in the interior of the brain, the surgeon must create a surgical corridor through healthy brain tissue to reach the desired location (Fig. 1B). The invasiveness of this approach can result in neurological deficits, prolonged hospital stays, and increased costs, including rehabilitation (*2*–*10*).

In general surgery, endoscopy is a common approach to reducing procedural invasiveness, but it is limited to locations in which the tip of the endoscope lies inside a gas- or fluid-filled cavity to enable visualization and tool motion. In the brain, endoscopic procedures can be performed inside the ventricles, a system of connected cavities filled with clear cerebrospinal fluid. Neurosurgical endoscopic instruments can considerably reduce morbidity compared with open surgery because they require only a small hole in the skull to insert the endoscope and create a small-diameter passage through the brain to reach the ventricles (Fig. 1, C and D). Current endoscopic technology can be used to effectively resect small, relatively avascular intraventricular lesions, but its limitations have precluded its use for the far more common larger, vascular lesions located around the ventricles (*11*–*16*).

Most neurosurgical endoscopes have a single tool channel, and the tools inserted through the channel have straight shafts. These characteristics force the surgeon to operate one-handed, and to produce lateral tool motion, the surgeon must pivot the entire endoscope trocar about its insertion point through the skull, leading to potentially damaging compression or disruption of the brain tissue along the trocar's length (Fig. 1D). To reduce these constraints, trocars with oval working channels have been developed (MINOP InVent, Aesculap) (*17*). With a 6.5 mm–by–3.7 mm oval working channel, however, lateral motion of 2-mm-diameter tools is limited to 4.5 mm if one tool is inserted or 2.5 mm if two tools are inserted.

Furthermore, no effective endoscopic technique exists for quickly locating and cauterizing bleeding vessels before the blood reduces or completely obscures visibility. When bleeding occurs, irrigation with warm saline is used to stop the bleeding and to clear the visual field. This approach can take tens of minutes to work and is only effective for small vessels. Hemorrhages can require the procedure to be aborted, and manipulating the tools and endoscope in an obscured field is extremely hazardous.

In contrast, the methodology of open surgery relies on the coordinated motion of two tools. To control bleeding, one tool can grasp and retract tissue to reveal the bleeding vessel while the second tool moves to cauterize it. To remove fibrous lesions that cannot be aspirated, one tool can grasp the tissue, enabling the second tool to cut it into pieces. To separate a lesion from surrounding healthy tissue, two tools can work together to gently dissect their boundary. When a blood vessel feeding the lesion is found on the boundary, one tool can retract the lesion while the second cauterizes the vessel.

[1]Department of Cardiac Surgery, Boston Children's Hospital, Harvard Medical School, Boston, MA 02115, USA. [2]Department of Neurosurgery, Hospital for Sick Children, University of Toronto, Toronto M5G1X8, Canada. [3]Department of Neurosurgery, Boston Children's Hospital, Harvard Medical School, Boston, MA 02115, USA.
*Corresponding author. Email: pierre.dupont@childrens.harvard.edu
†Present address: Boston Dynamics, Waltham, MA 02451, USA.
‡Present address: Vicarious Surgical, Waltham, MA 02451, USA.
§Present address: Department of Mechanical Engineering, University of Louisville, Louisville, KY 40292, USA.
¶Present address: Epic Systems, Verona, WI 53593, USA.

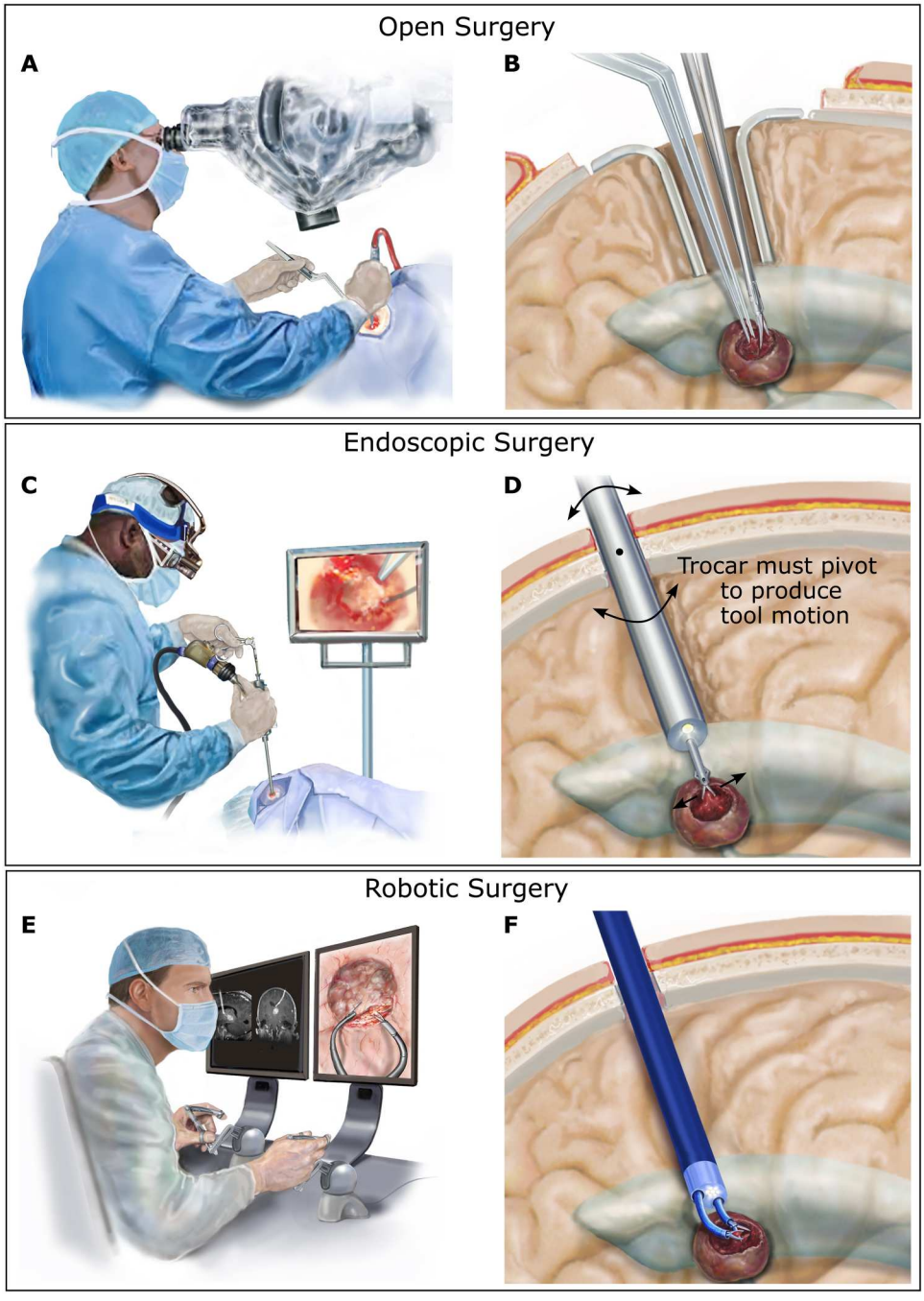

Fig. 1. Intracranial neurosurgery. (**A**) In open surgery, the surgeon views the brain through a microscope and uses both hands to manipulate tools inside the brain. (**B**) A portion of the skull is removed, and retractors are used to hold back healthy brain tissue to create a corridor through the brain to reach the tumor (shown in dark red) and to enable manipulation of the tools. (**C**) In endoscopic surgery, the surgeon inserts an endoscope trocar through the brain tissue to reach tumors adjacent to the fluid-filled ventricles. In most cases, only a single straight tool can be deployed through the trocar. (**D**) Endoscope insertion requires only a small burr hole in the skull and minimal disruption of brain tissue for insertion. To produce lateral motion of the tool, however, the endoscope trocar must be pivoted about the burr hole in the skull, causing potentially dangerous compression or disruption of the adjacent brain tissue. (**E**) Robotic endoscopic surgery enables the surgeon to sit comfortably while viewing the endoscopic video on a large screen and controlling the motions of two tools using joysticks. (**F**) As in standard endoscopy, the robotic trocar is inserted through a burr hole in the skull. Two tip-mounted steerable arms enable the surgeon to perform bimanual surgical tasks and to do so without pivoting the trocar against the surrounding brain tissue.

Robotics can enable a hybrid approach combining the reduced invasiveness of endoscopy with the bimanual capability of open surgery (Fig. 1, E and F). For such a system to expand the types of lesions that can be removed endoscopically, it should satisfy several clinical constraints. First, the robotic arms should have overlapping workspaces that are two to three times the diameter of the endoscopic trocar so that larger lesions can be accessed without pivoting the trocar (Fig. 1F). Second, because it increases risk to remove and reinsert an endoscope trocar into the brain, the system should be designed so that once it is inserted into the brain, it can remain inserted until completion of the procedure. This clinical constraint imposes several robot design constraints.

First, in open surgery, surgeons change the tools in their hands during a procedure. This requires that the robotic tools be designed so that they can be inserted and removed intraoperatively. For ease of use, enhanced safety, and reduced cost, it is preferable for tool swapping to be performed without removing or repositioning the robotic arms. For example, the arms may be positioned in a narrow deep cavity when a tool change is needed. It is both easier and safer to lock the arm in its current location during tool exchange rather than navigating it out of the brain, into the trocar, and then back into the cavity. With respect to cost, although the number of tool types is limited (such as forceps, scissors, and bipolar cautery), there are many variations in size and shape of each type. Depending on the task and tissue consistency, one design may be better suited than another, and the best choice can often change throughout the procedure. By separating the arms from the tools, costs are reduced because only a single set of arms is needed for the entire procedure rather than as many arms as tools.

Second, in endoscopic surgery, pieces of fibrous lesions are removed from the brain by grasping them with forceps and pulling them out through the working channel in the endoscope trocar. This is not an efficient way to remove large lesions. It is also impractical in a robotic system because it would likely require an assistant to manually remove the forceps from the robot, manually open the forceps to remove the tissue, manually close the forceps, reinsert the tool into the robotic system, and then potentially perform a wrist roll recalibration. The robotic system should therefore incorporate a means of removing tissue pieces from the brain that does not involve removing the arms and tools.

Last, the sterile components (arms, tools, and endoscopic trocar) should be designed as small compact modules that are separate from the drive system components (motors, bearings, and electronics) so that they can be easily sterilized. Compelling prior work in open robotic neurosurgery (*18*) and in robotic neuroendoscopy (*19*–*26*) has motivated us to create and evaluate a system that combines all of these features.

RESULTS

Bimanual robot design

We designed a two-armed endoscopic robot to meet these constraints (Fig. 2). The endoscopic trocar includes two arm channels, an optical channel, and an aspiration/irrigation channel (Fig. 2A). The 2.8-mm-diameter arms have trumpet-shaped workspaces that increase in diameter as the arms are extended from the trocar (Fig. 2B). When fully extended, the arms are 35 mm long and trace out circles that are also 35 mm in diameter (Fig. 2C). By rotating and translating the trocar about its axis, the overlapping workspaces of the two arms access a cylindrical workspace with a diameter of 43 mm. The arms are delivered through working channels with a center-to-center spacing of 8 mm. The endoscope is composed of a 4.2-mm-diameter chip camera with light-emitting diode (LED) illumination. To enable removal of fibrous tumor fragments, we included a 2.4-mm-diameter aspiration/irrigation channel. Its central location enabled either arm to feed tissue pieces into it for removal via aspiration. Allowing for angling of the camera, the resulting trocar cross section is 10 mm by 12 mm.

The robot (Fig. 2D) is composed of a drive system attached to an endoscopic trocar module, as well as arm modules (Fig. 2E) and tool modules (Fig. 2F). Each arm module has three degrees of freedom to position its tip in space. The tool modules provide a roll degree of freedom and a tool actuation degree of freedom, e.g., to open and close forceps. This set of degrees of freedom matches those available to a neurosurgeon during manual open surgery. This prototype design, based on adapting off-the-shelf tools and tubing (Fig. 2G), provided an effective platform for evaluating the potential of bimanual endoscopy and can ultimately be scaled to match the current diameter of clinical scopes of ~8 mm.

Viewing the endoscope video on a computer monitor (Fig. 2H), the operator controlled the robot arms using passive commercial input devices (Touch, 3D Systems) with attached custom tool controllers (Fig. 2I). Because neurosurgeons are accustomed to operating with little to no haptic feedback, it was not implemented in the robot. Input device position was mapped to robot arm tip position through a user-selected scaling factor. Tool controller roll angle and finger separation mapped to tool roll angle and open/close distance.

The drive system was mounted to a six–degree of freedom manual stage that currently clamps to a table but, in clinical use, would be cart mounted. The six–degree of freedom stage enables the robot to be positioned with respect to the patient. The drive system was designed to contain all the motors and linear transmission components so that it can be covered by a sterile drape (*27*). The sterile arm, tool, and endoscope modules could be attached to the drive system through mating inserts in the drape. This design also ensures that the arm, tool, and endoscope modules are very compact and easily sterilizable by steam or ethylene oxide.

Although almost all surgical robots use designs in which the tools are integrated into the robotic arms, we designed our tools to be separate modules that could be inserted and removed from an arm while it is extended from the endoscope trocar (Fig. 2F). This unconventional approach enhances both the efficiency and safety of intraoperative tool changing. When a tool change is needed, the arm can be positioned in a safe location near where the new tool will be used, and the tool can be changed with no need to interrupt surgical workflow.

For robustness, we also designed the robot arms as modules that can be changed intraoperatively (Fig. 2E). To allow for insertion and removal of tools, the robot arms must have a continuous lumen. The continuum robot designs that provide a continuous lumen use tendon actuation, multibackbone push-pull tendon actuation, or precurved superelastic concentric tubes (*28*, *29*). We selected the concentric tube design owing to its higher bending stiffness relative to diameter. As described in Materials and Methods, we optimized robot arm design by comparing the maximum workspace that could be achieved using arms composed of two and three tubes. This optimal design is composed of a concentric pair of precurved

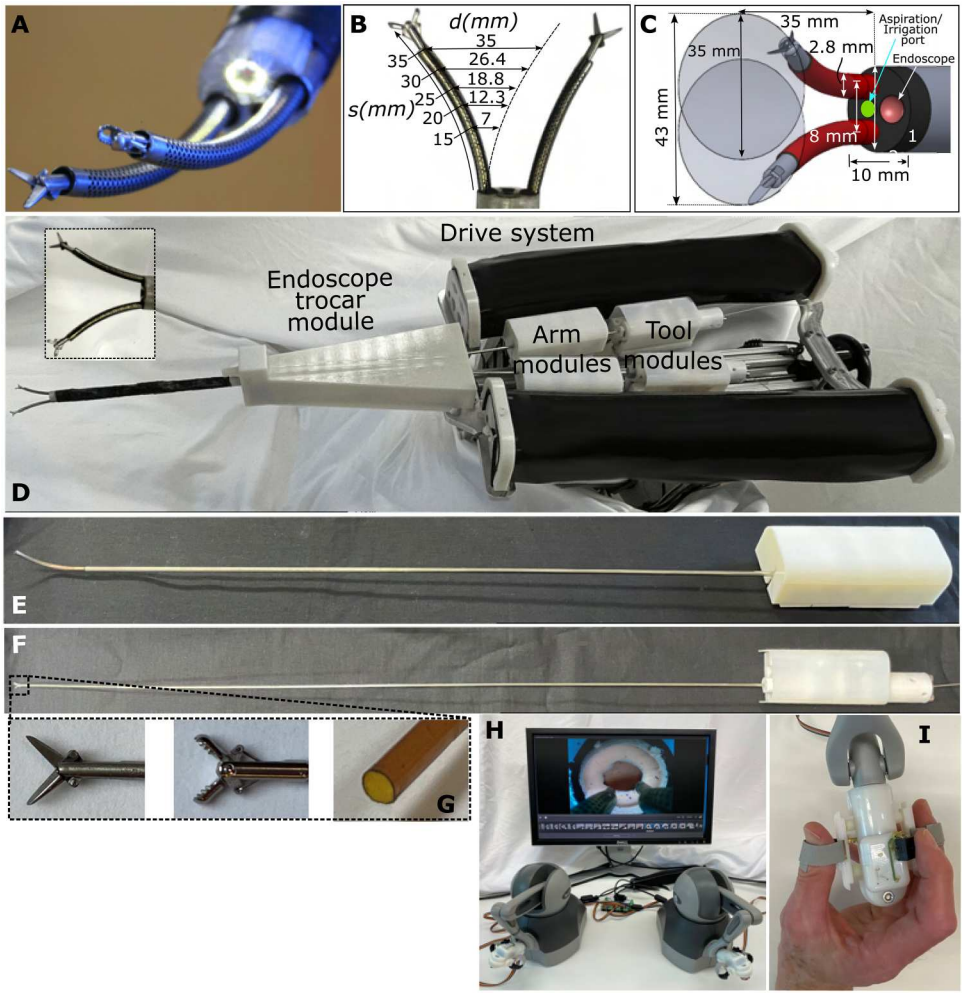

Fig. 2. Neuroendoscopic robot. (**A**) Tip of endoscopic trocar showing robotic arms with interchangeable tools. The endoscopic camera is surrounded by LEDs for illumination. (**B**) Arm workspace diameter, d, as a function of arm extension length, s, and bending radius of curvature, ρ, where $d = 2\rho[1 - \cos(s/\rho)]$. (**C**) Schematic showing dimensions of trocar and workspace of arms at full extension. An aspiration/irrigation port is included between the arms. (**D**) Robot is composed of an endoscopic trocar module, arm modules, tool modules, and a cart-mountable drive system. The system is designed so that a sterile plastic barrier (not shown) can be used to separate all the modules from the drive system (*27*). In this way, only the modules need to be sterile. Arm modules are inserted through the endoscope module. Tool modules are inserted through the arm modules. All modules are powered by transmission gears, which mate through the sterile barrier, with matching gears in the drive system as shown in fig. S2. (**E**) Arm module enabling independent rotation of the two precurved NiTi tubes comprising a robotic arm. (**F**) Tool module that can be changed intraoperatively. (**G**) Tool tips showing (from left to right) scissors, forceps, and an aspiration/irrigation tool. (**H**) The surgical console is composed of a computer monitor and two mechanical joysticks. (**I**) Custom tool controllers enable the surgeon to precisely open and close scissors and forceps. A push button on the controllers pauses and restarts robot motion.

superelastic NiTi tubes with a trumpet-shaped workspace as shown in Fig. 2B. The curvatures and relative stiffnesses of the tubes are designed so that the arm is straight when the tubes are rotated such that the individual precurvatures oppose each other (*30*, *31*). The arm achieves maximum curvature when the tubes are rotated so that the precurvatures are aligned.

Although superelastic NiTi remains elastic up to about 10% strain, the precurvature of previously reported concentric tube robots has been limited to a maximum of about 4% maximum strain in bending [approximated by tube outer radius divided by bending radius of curvature (*31*)] because higher strains cause the tubes to buckle during the precurving process (*32*). In addition, because strains in NiTi above 1% are nonlinear, it was previously difficult to design a pair of high-curvature tubes that would become perfectly straight above 1% strain (*32*). These constraints limited the diameter of the workspace that could be produced by a balanced-stiffness tube pair. To overcome these limitations, we developed a tube patterning process that enabled us to increase balanced stiffness robot arm curvature from 1 to 4.5% strain (computed as if the tube was unpatterned). This increases the arm workspace diameter from 9 to 35 mm at our maximum arm extension length of 35 mm (Fig. 2B). The resulting arm workspace diameter as a function of arm extension length is given in Fig. 2B.

We created robotic forceps and scissors by modifying existing manual flexible endoscopic instruments. We selected instruments with straight but sufficiently flexible shafts so that they would not change the curvature of the robot arms when inserted inside them. We replaced the handles with drive modules that provided for a roll

degree of freedom and the capability to open and close the tool via a push/pull wire (Fig. 2F, 2G). We also designed an aspiration and irrigation tool composed of a polyamide tube that could be inserted through the robotic arm so that its tip was flush with the tip of the arm. The tube module was connected to a pump-driven aspiration and irrigation circuit. Under foot pedal control, aspiration can be used for sucking out soft tumors, whereas irrigation can be used to clear the field of view or to unplug the tube if it becomes plugged during aspiration.

Defining neurosurgical skill tasks

To assess the value of the robot in performing neurosurgical procedures, we first analyzed the surgical workflow of open brain tumor resection (Fig. 1A). As shown in Fig. 3, it is composed of a sequence of three fundamental tasks. First, the boundaries of the tumor are identified by gently separating it from the surrounding brain tissue around its top edge (Fig. 3A). This step involves locating, cauterizing, and cutting any blood vessels feeding the tumor. Separation can only be performed to a limited depth because the tumor and brain are pressed against each other. To create additional separation, a window into the tumor is created by cutting an opening in the outer layer or capsule of the tumor (Fig. 3B). The surgeon then begins removing the contents of the tumor in a process known as debulking while again being careful to locate and cauterize blood vessels (Fig. 3C). Some tumors are soft enough that they can be removed using aspiration. Other tumors are fibrous; they must be removed piece by piece. Debulking the top of the tumor creates space for the walls of the tumor to collapse inward. This enables the surgeon to return to the task of Fig. 3A to deepen the separation between the brain and the tumor at its boundaries. The surgeon then alternates between boundary separation and debulking until the entire tumor is removed.

On the basis of this analysis of open tumor resection, we defined a set of four skill tasks (Fig. 4, A to D) intended to capture the coordinated tool manipulations used to perform the three fundamental tumor removal tasks (Fig. 3). The first three skill tasks directly represent the three tumor removal tasks. The boundary separation task (Fig. 4A) required the surgeon to peel back a phantom tumor capsule from the surrounding brain phantom to locate, cauterize, and cut four blood vessels positioned around the tumor. The capsule cutting task (Fig. 4B) involved accurately cutting a circular hole in a capsule phantom. In the fibrous tumor debulking task (Fig. 4C), the surgeon must remove the body of a tumor phantom by tearing off small pieces from inside a phantom capsule and removing them from the brain phantom. Because visualization is especially challenging in endoscopic procedures, we also defined a fourth skill task, hidden ring transfer (Fig. 4D). This task was directed at assessing the capability to coordinate arm motions to simultaneously visualize and manipulate tissue.

Comparing robotic and manual endoscopic surgery using skill tasks

Physical and computer-based skill tasks are often used in medical education to train and compare the capability of an individual surgeon with a baseline performance level to certify them in the use of complex medical equipment in a simulated surgical environment (*33*–*37*). Here, we used skill tasks to compare how alternative medical devices affect surgeon proficiency (*38*, *39*). Specifically, we constructed a manual endoscope system with trocar dimensions, optics, and tools matching those of the robotic system. We then conducted experiments comparing the performance of an operator using the robotic and manual endoscopic devices. For skill tasks one to three, data (n = 5) were collected from a single expert operator (P.E.D.). For the fourth task, data were collected from the expert operator and from two neurosurgeons (S.S. and J.D.). All experiments were performed in P.E.D.'s laboratory at Boston Children's Hospital, Boston, MA, USA.

Each neurosurgeon was trained to perform each task using the manual system and the robotic system. Training consisted of task demonstration and explanation by an expert user. This was followed by the operator performing a minimum of five training trials with verbal feedback provided by the expert user. Training was considered complete when the operator agreed that they felt comfortable performing the task. The operator then performed a sequence of trials (minimum of five trials), and the data from these trials were collected for comparison. The order in which manual and robotic testing was performed for each was randomly selected. All tasks

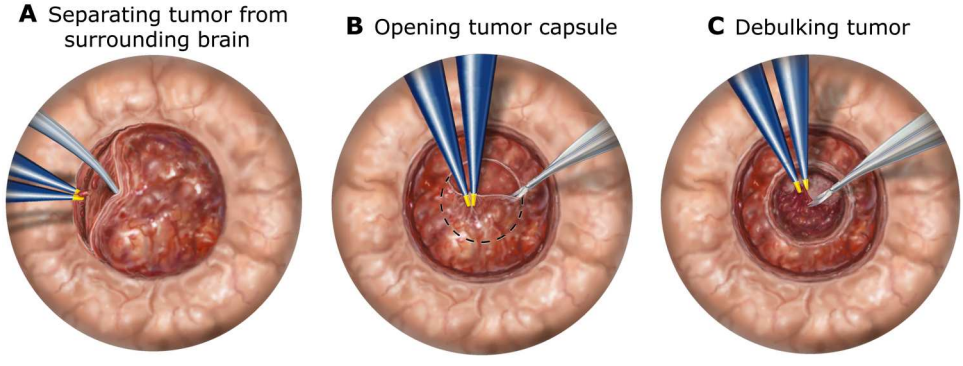

Fig. 3. Steps of brain tumor resection. (**A**) The first step to removing a tumor is to carefully start separating its boundaries from the surrounding brain tissue. The goal is to locate, cauterize, and then cut blood vessels feeding the tumor. Because the tumor is pressing against the surrounding brain, only a little separation is usually possible at the start. To create more room, the following steps have to be performed. (**B**) Tumors and cysts typically have an outer membrane or capsule. A window is cut in the capsule to provide access to the contents of the tumor. (**C**) Tumor debulking, in which the contents of the tumor are resected, must be done carefully so that blood vessels can be located and cauterized. Once the top of the tumor has been resected, its walls begin to collapse inward. At this point, the surgeon returns to step (A) and deepens the separation between the tumor and the surrounding brain. The surgeon then continues to alternate between steps (A) and (C) until the entire tumor is removed.

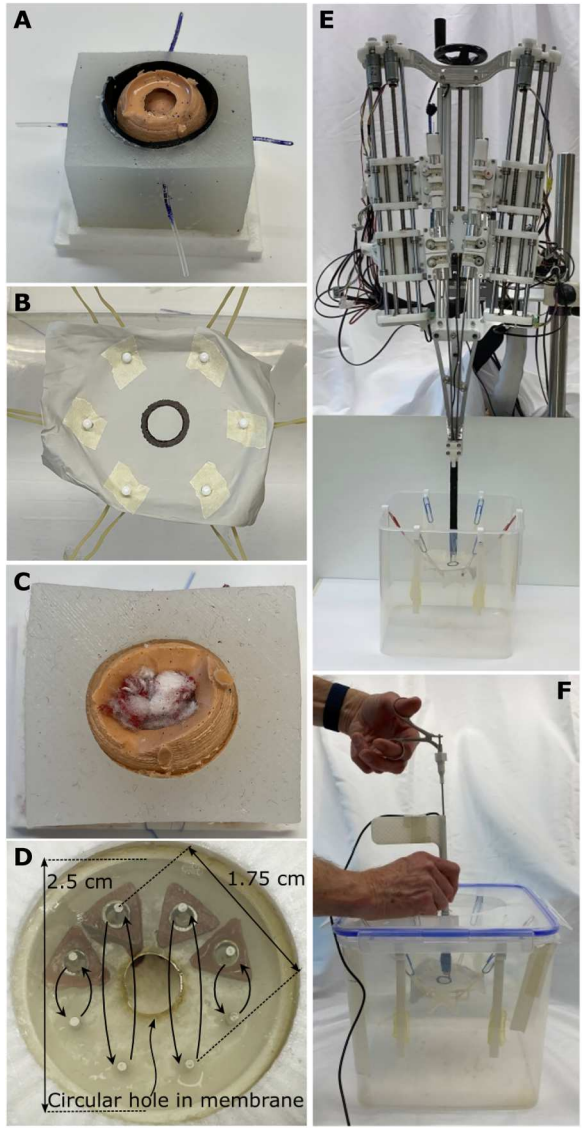

Fig. 4. Fundamentals of neurosurgery skill tasks. (**A**) Boundary separation (skill task 1). The goal was to search between the olive-sized tumor and surrounding brain to locate four tubes representing blood vessels. The vessels were first cauterized with forceps and then cut with scissors. The task was to be performed without putting pressure on the surrounding brain surface, composed of a black conductive polymer enabling measurement of tool contact time. This is an inherently bimanual task because one tool is needed to retract the tumor while the second cauterizes and cuts the blood vessel. (**B**) Capsule cutting (skill task 2). The goal was to cut out a circular window in a polymer sheet while staying inside the black circle boundary. The polymer sheet was mounted on a soft suspension of rubber bands to simulate the compliance of brain tissue. In robotic operation, one arm was used to position and tense the membrane to facilitate cutting by the second arm. (**C**) Fibrous tumor debulking (skill task 3). The goal was to remove the tumor contents composed of seven small balls of cotton suspended inside the silicone tumor capsule on suture. To remove each ball from its suture attachment, it had to be torn into pieces. In manual operation, each piece was pulled out by the tool through the trocar. In robotic operation, the arms fed the pieces into an aspiration port for removal. (**D**) Hidden ring transfer (skill task 4). This task evaluated bimanual dexterity and visualization. Four triangular rings and eight pegs were hidden behind an opaque membrane (shown semitransparent here) with a 6-mm-diameter hole in its center. The goal was to move each ring between corresponding top and bottom pegs. In manual operation, the trocar had to be used to pull back the membrane to see the rings and pegs. In robotic operation, one arm could pull back the membrane while the other moved the rings. (**E**) Robotic skill testing. The robot is positioned above water tank holding each skill task. (**F**) Manual skill testing. The operator uses manual trocar and tools in an identical water tank.

were performed in a water tank to simulate immersion in cerebrospinal fluid. Each task is described below.

Boundary separation (skill task 1)

The model consisted of a partially debulked silicone tumor capsule surrounded by silicone brain tissue that is lined by a conductive polymer layer. Tool contact with the conductive polymer was detected electrically, and the number of contact episodes along with their duration was recorded. Four phantom blood vessels made from 0.9-mm-diameter silicone tubing coated with blue paint were positioned midway down the capsule and about 90° apart. The task was composed of locating the blood vessels by pushing the capsule wall inward while avoiding contact and compression of the surrounding brain. When a blood vessel was located, standard forceps (simulating bipolar cautery forceps) were used to grasp it. By shaking or sliding the forceps on the vessel, blue paint was removed, which marked the cautery location. After cautery, scissors were then used to cut the vessel downstream of the cauterization. The metrics used to evaluate task performance were maximum pivoting angle of the trocar, duration of brain contact, number of vessels successfully cauterized and cut, tool visualization during cauterization, and completion time.

When performing the task manually (Fig. 5A and (movie S1), the forceps were inserted through the instrument channel, and by levering the trocar, the tumor capsule was retracted to search for a blood vessel. Once a vessel was located, the forceps fingers could be oriented tangent to the capsule surface to grasp the vessel. Care had to be taken not to cauterize adjacent to the capsule to leave room to cut the vessel downstream of the cauterization. The forceps were then removed from the trocar and replaced with scissors. The vessel was relocated by capsule retraction using the shaft of the scissors, and the vessel was cut. With the camera positioned above the tool channel in the trocar, visualization was best for the vessels located on the left and right sides of the capsule. The trocar could then be rotated 90° to reach the remaining two vessels.

This task was performed robotically using forceps in one arm and scissors in the other (Fig. 5B and movie S2). The best approach was to use the two arms to "walk" down the top outer surface of the

Fig. 5. Comparison of manual and robotic skill task performance. (**A** and **B**) Boundary separation (skill task 1). (A) Manual separation (movie S1). The operator used forceps to pull back the tumor capsule. Once a blood vessel tube was located, the forceps were used to squeeze the tube to simulate cautery. The forceps were then exchanged for scissors to cut the vessel. With a single tool, it was extremely difficult to visualize the vessel while cauterizing and cutting it. (B) Robotic separation (movie S2). One arm was used to pull back the tumor capsule while the second cauterized and cut the vessel. (**C** and **D**) Capsule cutting (skill task 2). (C) Manual cutting (movie S3). The operator pivoted the trocar to move around the circle during cutting. Cutting became more difficult as the task progressed because of reduced tension in the circular target. (D) Robotic cutting (movie S4). One arm was used to position and tense the membrane while the second arm cut it. Bimanual tensioning and cutting of tissue are a standard neurosurgical technique. (**E** and **F**) Fibrous debulking (skill task 3). (E) Manual debulking (movie S5). The operator tore off each piece and, while grasping it, pulled it out through the trocar. Tumor pieces can be lost if they cannot fit through the trocar. Visibility is also challenging around the periphery. (F) Robotic debulking (movie S6). One arm held open the capsule while the second arm tore off a tumor piece and fed it into the aspiration tube located between the arms. (**G** and **H**) Hidden ring transfer (skill task 4). (G) Manual transfer (movie S7). The trocar had to be inserted through the hole in the membrane to enable visualization. The challenge was that the membrane could easily slip off the trocar. Note that the ring accidentally knocked off the peg at the end of the movie. (H) Robotic transfer (movie S8). As shown, the left arm pulled back the membrane to enable visualization, whereas the right grasped and moved the ring.

tumor capsule looking for blood vessels. When one was located, the scissors arm held back the capsule while the forceps arm grasped it to simulate cauterization. The forceps arm then took over holding back the capsule while the scissors arm was used to cut the vessel on the tumor side of the cauterization site. Because the user knew that the vessels were located 90° apart, it was easiest to now move to the bottom edge. After cutting that vessel, it was fastest to rotate the trocar 90° to provide the best approach for the remaining two vessels.

This is a bimanual task. One tool was needed to hold back the tumor for visualization and to create a working space for the second tool to perform cauterization and cutting. As shown in Fig. 5A and movie S1, although it was possible to cauterize and cut all the vessels, attempting the task with one tool resulted in extremely

poor visualization. Furthermore, it was not possible using one tool to ensure that the vessel was cut downstream from where it was cauterized. Cutting upstream would result in uncontrolled bleeding. For both reasons, this would not be considered safe to perform manually. In contrast, using two robotic arms (movie S2) makes the task easy to perform. As shown in Fig. 6A, mean completion time was reduced by almost a factor of 3 from 305 to 114 s, and mean brain contact time was reduced by a factor of 10 from 102 to 10 s per trial. Furthermore, the robotic trocar remained stationary during all trials while the manual trocar pivoted ±6° in both horizontal coordinate directions, corresponding to a trocar tip motion of ±9 mm (Fig. 6B).

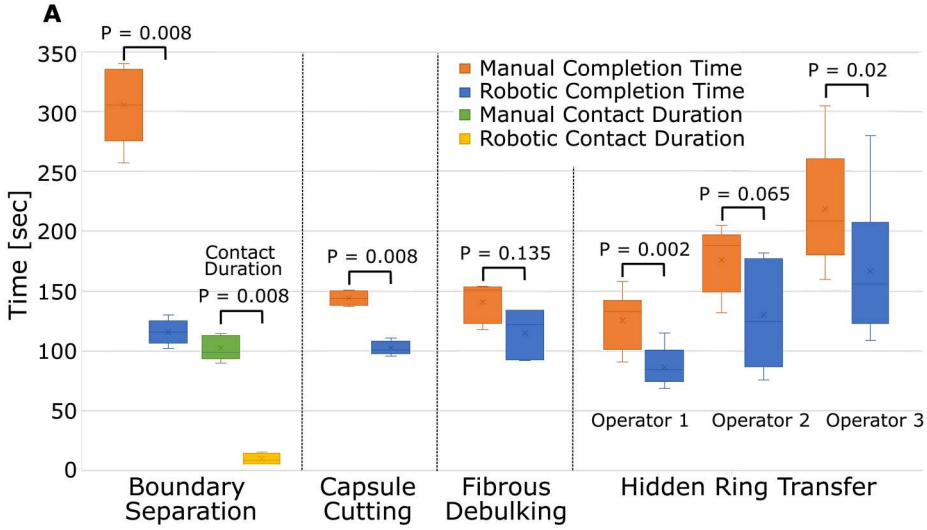

B

	Trocar Pivoting Angle [deg]	
Task	Manual	Robotic
Boundary Separation	± 6	0
Capsule Cutting	± 11	0
Fibrous Debulking	± 6	0
Hidden Ring Transfer	± 4	0
	Trocar Tip Displacement [mm]	
	Manual	Robotic
Boundary Separation	± 9	0
Capsule Cutting	± 8	0
Fibrous Debulking	± 9	0
Hidden Ring Transfer	± 7	0

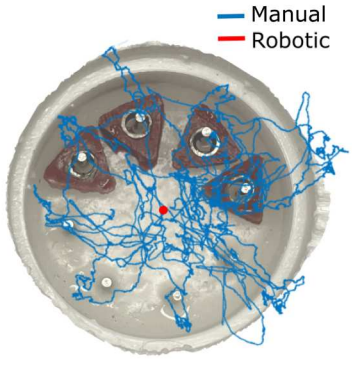

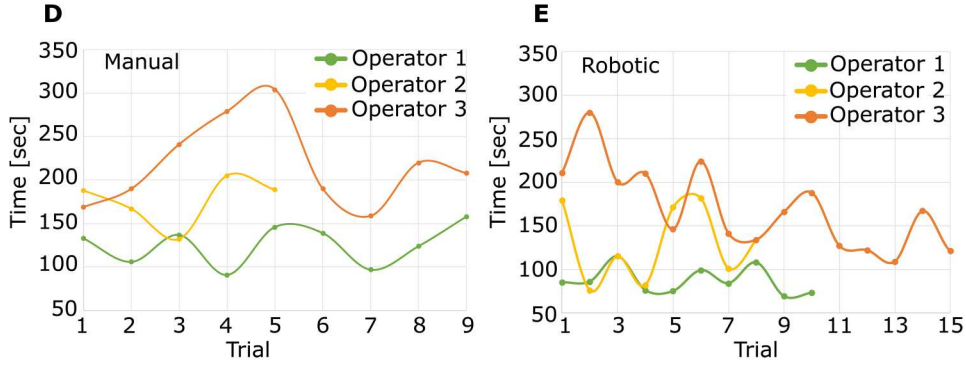

Fig. 6. Skill task results. (**A**) Comparison of manual and robotic completion times for the four neurosurgical skill tasks. For boundary separation (Task 1), brain contact time is also compared. For ring transfer, the performance of three operators is compared. (**B**) Comparison of manual and robotic trocar pivoting for the four skill tasks. Trocar displacement compresses and can tear brain tissue surrounding trocar. (**C**) Example trocar tip path during hidden ring transfer measured using a trocar-mounted electromagnetic sensor. (**D**) Manual hidden ring transfer time versus trial number for three operators. (**E**) Robotic hidden ring transfer time versus trial number for three operators.

Capsule cutting (skill task 2)

The goal of this task was to cut out a 2-cm-diameter circular target from a rubber membrane and to remove the target from the tank. The membrane was held taut in a frame, but the frame was attached to the tank by a soft elastic mount. The border of the target circle was 3 mm wide, and all cutting must be made inside the border. The metrics used to evaluate task performance were ability to complete the task, maximum pivoting of the trocar, and completion time.

Performing the task manually (Fig. 5C and movie S3), scissors were inserted through the instrument channel, and the trocar was pivoted about a burr hole in the lid of the test tank (Fig. 4F) to move the scissors around the perimeter, making sequential connected cuts. When the circle was almost completely cut out, the user could exchange the scissors for forceps to grasp, tear off, and remove the circular target.

This task was performed robotically with scissors in one arm and forceps in the other (Fig. 5D and movie S4). With the scissors on the right, the arms (with tools closed) were first used to walk the membrane to the right so that the left side of the circle was centered in the visual field. The left arm then held the circle in position while the scissors in the right arm were used to cut the circle along the curve between the clock positions of about 7:30 to 10:30. Once this portion was cut, the left arm forceps grasped the circular target inside the cut region to provide tension on the target circle while the right scissors cut along the remainder of the boundary. The circular target, still held in the left forceps, was then removed through the arm by removing the tool module.

For most trials, this task was successfully performed manually and robotically. In several manual trials, the circular cutout curled underneath the suspended membrane while still attached to the membrane. In this position, it was impossible to grasp, so the cutout could not be removed. In the robotic trials, one arm was always grasping the cutout, so it was always possible to remove it. Because this curling appeared to occur randomly, we do not report statistics on it. Robotic operation reduced completion time by 40% (Fig. 6A) and eliminated the manual trocar pivoting of ±11° in both horizontal coordinate directions, corresponding to a trocar tip motion of ±8 mm (Fig. 6B).

Fibrous tumor debulking (skill task 3)

A fibrous tumor was modeled using seven pieces of cotton fiber (about 5 mm on a side) that were suspended inside a silicone tumor capsule using lengths of polymer suture that passed through the fiber and the capsule. The goal of the task was to remove all of the phantom tumor from the capsule by tearing apart the pieces. The cotton pieces were sufficiently fibrous that they could not be removed by aspiration. Furthermore, grasping and pulling on a piece would tear off a small portion but did not remove the entire piece. The metrics used to evaluate task performance were complete removal of tumor debris, tool visualization, completion time, and maximum pivoting angle of trocar.

Performing the task manually (Fig. 5E and movie S5), forceps were inserted through the instrument channel, and the trocar was pivoted about the burr hole in the test tank lid (Fig. 4F) to grasp the phantom tumor tissue. To remove the tissue from the brain, the forceps were retracted through the instrument channel while continuing to grasp the tumor fragment. The piece was then removed from the forceps, and the forceps were reinserted through the instrument channel to tear off the next piece. This was repeated until visual inspection showed that all tumor tissue had been removed.

This task was performed robotically with forceps inserted through both arms and an aspiration tube extended between the arms (Fig. 5F and movie S6). The aspiration tube acted as a "mouth" into which tumor tissue could be fed by the two arms. The arms were used in tandem, with one holding back the capsule while the other tore off a piece of cotton fiber. If the torn piece was small, then it could be fed directly into the aspiration tube. If the piece was large, the two arms were used to tear it into smaller pieces before feeding it into the aspiration tube. In actual surgery, bipolar cautery forceps would be used as one hand to enable rapid cauterization if a blood vessel was found during debulking.

Because the circular window in the tumor capsule was small, some tumor pieces had to be grasped blindly during manual removal. In contrast, the second robotic arm was able to hold back the capsule so that robotic debulking was performed under consistent visualization. In addition, when removing tumor pieces manually, the grasped piece was sometimes too large to fit through the working channel, so portions broke off when the tool was removed. These pieces sometimes floated away because the tool was not available while it was being pulled out to immediately grasp them. In contrast, the robotic arms were able to efficiently feed tumor pieces into the aspiration tube for removal. The suction force at the tube tip drew in nearby pieces, reducing the chances of their escape. Although completion time was similar for manual and robotic performance (mean times of 141 and 115 s, respectively, Fig. 6A), no pivoting of the robotic trocar was needed despite its improved visualization. The manual trocar tip pivoted through ±6° in the horizontal coordinate directions or ±9 mm (Fig. 6B).

Hidden ring transfer (skill task 4)

Eight pegs were arranged so that they were hidden behind an opaque silicone membrane that has a 6-mm-diameter hole in its center. Four rings were placed on the top four pegs. The goal of the task was to sequentially move the four rings to the corresponding bottom pegs and then to move them back again. The operator was allowed to move the rings either from right to left or left to right. The metrics used to evaluate task performance were the number of rings dropped or placed on the wrong peg, maximum pivoting angle of trocar, and completion time.

When performing the task manually (Fig. 5G and movie S7), to see the pegs and rings, the trocar must be inserted through the circular hole in the membrane and then pivoted to pull back the membrane in the desired direction. Forceps inserted through the instrument channel were used to grasp a ring. Trocar pivoting was used to align the forceps to pick and place the rings. The insertion depth of the trocar through the membrane had to be carefully maintained because visualization was lost if the trocar slipped out of the membrane hole.

This task was performed robotically using forceps as both hands (Fig. 5H and movie S8). For pegs to the left of center, the left arm was used to pull back the membrane to locate each peg and ring. The right arm was then used to grasp and move the ring. For pegs to the right of center, the right arm pulled back the membrane and the left arm moved the ring.

The main challenge of manual task performance was that it was very easy for the trocar to slip out of the hole in the membrane,

leading to loss of visualization of the tool. If the tool was grasping a ring when the trocar slipped out, the tool could not be withdrawn into the trocar during reinsertion without dropping the ring. When a ring was dropped, it was often harder to pick up again. If the operator continued to hold a ring while reinserting the trocar, it could knock other rings off their pegs during reinsertion. In contrast, bimanual robotic task performance was straightforward because the membrane retraction and ring handling subtasks were decoupled; they were handled by separate arms. This task was performed by one expert operator (operator 1) and two neurosurgeons (operators 2 and 3).

As seen in Fig. 6A, two of three operators were statistically faster (30 and 27% faster) at performing the task with the robot. Operator 2 was 26% faster with the robot, but owing to a large variance in robotic task times, this was not statistically significant. Although operator 3 had the longest completion times, they also had the lowest mean ring drop and misplacement rates per trial: (0.1 manual, 0.3 robotic) versus (1.2 manual, 0.4 robotic) for operator 1 and (1.2 manual, 1.3 robotic) for operator 2.

To investigate whether continued learning was occurring during the recorded trials, trial time versus trial number was plotted in Fig. 6 (D and E). As expected from the plot of Fig. 2A, variation in trial time was smallest for expert operator 1, who had extensive experience with both the manual and robotic systems. In contrast, the plots of Fig. 6 (D and E) suggest that operator 3 was still learning during both manual and robotic task performance. In manual operation (Fig. 6D), trial time increased over the first five trials before coming back down. This suggests that operator 3 was still experimenting with their technique in the early trials. In contrast, their robotic task data suggest a steady increase in proficiency over the course of their trials. Operator 2, who was not statistically faster with the robot, was consistent on a trial-to-trial basis for the manual task. Their robotic times, however, varied widely, suggesting that they were still learning and, with practice, could converge to the performance of operator 1.

None of the operators required pivoting of the robotic trocar to complete the task. Manual task performance required pivoting for all operators through ±4° in the two horizontal coordinate directions, equating to ±7 mm (Fig. 6B). To illustrate manual pivoting, an electromagnetic tracker (Ascension trakSTAR) was attached to the manual endoscope trocar. A typical manual trocar tip path is plotted in Fig. 6C.

Pineal tumor debulking

In addition to the skill tasks, we also investigated the robot in the context of a specific procedure that is currently too difficult to perform endoscopically. Pineal tumors originate in the pineal gland located in the center of the brain in a region surrounded by major blood vessels and critically important brain structures (Fig. 7). Although tumor grading can be performed by endoscopic biopsy (Fig. 7B), tumor resection is typically performed as open surgery to provide access to the entire tumor and to allow for timely control of bleeding (Fig. 7A). To explore whether the robot could enable endoscopic tumor resection as shown in Fig. 7C, we constructed a phantom brain model using medical images of a patient with a pineal tumor (Fig. 7, D to F). We constructed pineal tumor phantoms using a silicone capsule filled with banana and sealed with 0.1-mm-thick polyvinylidene chloride (PVC) film (Polyvinyl Films Inc.). The banana core was comparable in consistency to nonfibrous tumor tissue and could be aspirated. The PVC film was selected to model a front capsule surface that could be ruptured with forceps or scissors. The phantom tumor was positioned inside the brain model in a water tank for testing (Fig. 7D). We then compared manual and robotic tumor debulking. The endoscope trocar was introduced using an anterior transcortical approach into the left lateral ventricle and up to the foramen of Monro to reach the tumor, which was extending into the third ventricle (Fig. 7, B to F). The tumor was partially hidden from view by the wall of the foramen of Monro and the roof of the third ventricle.

In manual debulking (Fig. 8A and movie S9), the forceps were first used to grasp and tear open the plastic wrap forming the top surface of the tumor capsule. The forceps were then exchanged for an aspiration tube that was used to suck out the capsule contents. The challenge of the task was that the operator wanted to visualize what they were about to aspirate to locate and cauterize any blood vessels. Because it was not possible to advance the trocar further, however, the straight aspiration tool had to be used to retract brain tissue to access the entire tumor.

Robotically, this task was performed using forceps as the left hand and an aspiration tube as the right hand (Fig. 8B and movie S10). In clinical use, the forceps would be bipolar cautery forceps. After tearing open the capsule with the forceps, the left hand was used to retract brain tissue and to reposition the capsule to provide complete visualization of tumor aspiration.

In comparison with hidden ring transfer (skill task 4), pineal tumor resection is more challenging because, owing to the delicate nature of the tissue surrounding the foramen of Monro, the trocar cannot be forced into and levered against the foramen of Monro to provide an unobstructed view of the tumor capsule. Consequently, the task is comparable to that of boundary separation (skill task 1), where it was found that it is difficult for a single straight tool to simultaneously perform two functions: in this case, delicate retraction of normal brain tissue and aspiration of tumor tissue. In attempting to do both, safe visualization is lost, which can easily lead to tearing of a blood vessel. With a single tool, it would not be possible to control bleeding by immediate use of bipolar cautery because the blood would obscure the visual field faster than the aspiration tube could be swapped for bipolar forceps. Alternatively, the second arm of the robotic system provides this capability while also reducing the risk of bleeding by enabling better visualization via tissue retraction. Manual and robotic mean completion times were comparable (92 and 87 s). As with the four skill tasks, no pivoting of the robotic trocar was needed, while the manual trocar was pivoted through ±5° in the plane perpendicular to the trocar (±6 mm).

DISCUSSION

An enduring challenge in medical robotics is to demonstrate that robotic assistance truly adds value when compared with traditional manual instruments. By defining a set of fundamental neuroendoscopic tasks associated with lesion resection, we were able to determine the benefits of bimanual robotic assistance compared with current manual endoscopic technology. We have also demonstrated how pineal region tumor resection, a procedure most often performed now using open surgery, has the potential of being performed endoscopically using robotic assistance.

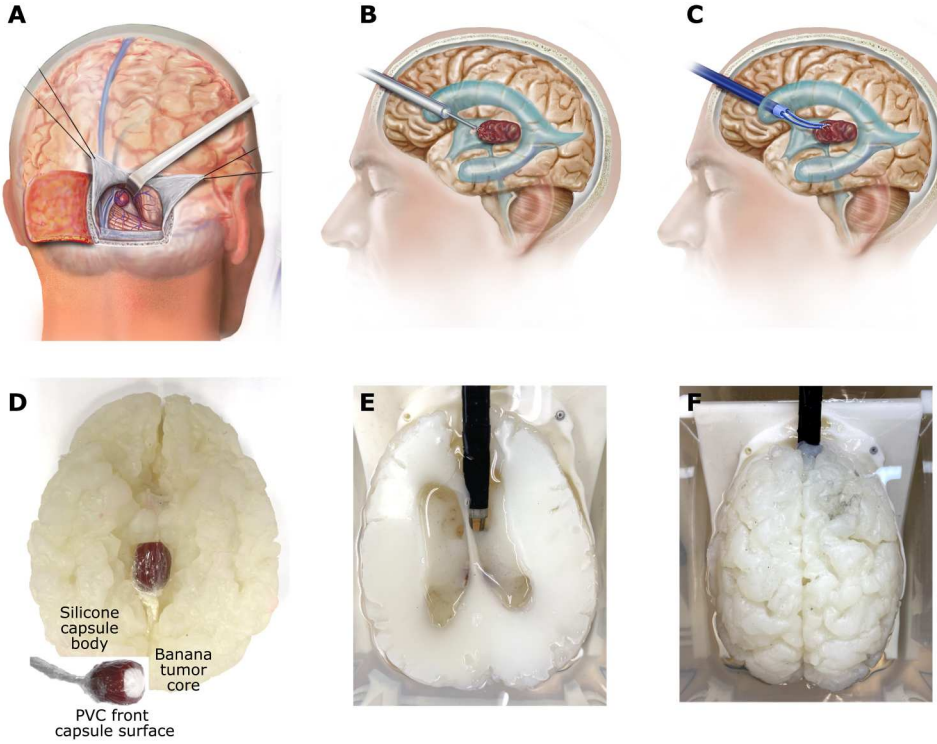

Fig. 7. Pineal tumor debulking task in phantom brain model. (**A**) Occipital transtentorial approach for open resection of a pineal tumor. The occipital lobe is retracted to reach the center of the brain. (**B**) The standard endoscope is typically used only to biopsy a pineal tumor because it does not provide sufficient steerability to reach the entire tumor. (**C**) The bimanual robotic endoscope provides the capability to visualize and reach along a curved path to safely access the entire tumor. (**D** to **F**) Silicone model of patient with enlarged ventricles due to hydrocephalus. (D) Bottom view showing phantom tumor extending from the region of pineal gland into third ventricle. The inset shows tumor construction. The banana filling tumor capsule is slightly fibrous but can be removed by aspiration. (E) Top view showing the robot entering the right lateral ventricle with arms extending through foramen of Monro into the third ventricle to access the tumor. The goal of the task is to open and entirely debulk the capsule by aspiration under continuous visualization. Manual tumor resection was performed using the same angle of entry. (F) Top view of the entire brain phantom.

We identified two primary benefits of a robotic bimanual endoscope system. First, each steerable arm can access a trumpet-shaped workspace volume that increases in diameter as the arm is extended (Fig. 2B). This provides a large working volume at the trocar tip and the ability to work off-axis from the trocar. With this workspace, we were able to robotically perform the four skill tasks and the pineal phantom tumor resection without any brain-compressing and potentially tissue-tearing pivoting of the trocar. This capability could enable neurosurgeons to work around corners and to endoscopically resect larger tumors that they would currently remove using open surgical techniques.

The second primary benefit of the robotic system revealed through our testing is that neurosurgery is composed of fundamentally bimanual tasks. For example, many tasks require the first hand to be used exclusively to retract tissue to enable visualization and to provide open space for the second hand to cauterize, cut, or aspirate tissue (skill tasks 1, 3, and 4; pineal tumor debulking). In contrast, the manual technique of using the trocar tip for retraction involves brain compression and suffers from coupling of the retraction and tool motions. A second bimanual task element that we identified is the use of the first hand to position or tension tissue so that it can be cut off (skill task 2). This capability enables more precise and thus safer tissue resection. A third advantage of bimanual systems is the continuous availability of a second tool to handle contingencies. This includes maintaining control of tissue and tumor debris so that it does not float out of reach (skill tasks 2 and 3). Most important, it allows the surgeon to always have bipolar cautery forceps at the ready, both to cauterize blood vessels as they are located during boundary creation and debulking and to stop bleeding from tumor vessels that are disrupted or cut.

The prototype robotic system used to demonstrate these benefits incorporates several features that will facilitate clinical translation. First, the tools and arms were designed as independent modular components. Most robots are not designed this way because it is easier to fabricate integrated arms and tools. By designing them as separate modules, however, the surgeon can change tools intraoperatively without removing the arms or trocar from the brain. If an arm has been delicately navigated into position inside the brain, there is no need to move it or to recalibrate it when changing tools. Furthermore, with the tool and arm modules designed as disposables containing the minimum mechanical and electrical components, procedural costs are reduced because a new set of arm tubes is not used with every tool. The modules are also small and light enough to be easily sterilized, shipped, and physically handled by operating room staff.

We also introduced the use of laser-patterned tubes to increase the precurvature of concentric tube robots. Specifically, we were able to increase the precurvature in a stiffness-balanced pair of tubes from 1 to 4.5% (nominal bending strain in the outer tube). For an extension length of 15 mm, this increased the arm workspace

Fig. 8. Comparison of manual and robotic pineal tumor debulking. (**A**) Manual tumor debulking (movie S9). Forceps were first used to create a hole in the plastic membrane. Then, an aspiration tube was used to debulk the capsule. Note that the left side of the capsule was aspirated blindly because it could not be visualized. This could not be done safely in practice because the region may contain blood vessels. (**B**) Robotic debulking (movie S10). In robotic debulking, the left arm was used to retract tissue and to reposition the capsule, enabling continuous visualization during aspiration. (**C**) Comparison of manual (n = 5) and robotic (n = 3) debulking times.

diameter from 1.6 to 7 mm. Put another way, to get a 7-mm-diameter workspace at 1% strain, the arm would have to be extended over twice as far to 31 mm instead of 15 mm. This enhanced workspace, in combination with the addition of an aspiration mouth between the two arms, provides the potential to robotically remove large fibrous tumors very efficiently.

Although endoscopy in the ventricular system has been considered here, the robotic technology may be applicable in other neurosurgical contexts. For example, to reduce the invasiveness of some open-brain surgeries, a small-diameter cylindrical sheath is sometimes used to create a path to a tumor located in solid brain tissue. The sheath creates a narrow working space for manipulating manual tools. A bimanual endoscopic robot would likely provide visualization and manipulation advantages over the current approach. Similarly, the robotic system could be adapted to performing transsphenoidal and spinal procedures. If these tasks require arms with more degrees of freedom or different types of tools, the modular system can be easily adapted to meet these needs.

The concept of using skill tasks for surgeon training and assessment on specific medical devices is well established and thoroughly validated. In contrast to cadaver studies and in vivo animal studies, skill tasks have the advantages of being inexpensive and easily reproducible. This enables the tests to be performed many times to allow for training and for statistical comparison. Examples include the Fundamentals of Laparoscopic Surgery curriculum (*33*, *36*), its extension to robotic laparoscopic surgery (*35*), and the Fundamentals of Endoscopic Surgery, focusing on the use of manual flexible endoscopic instruments in the gastrointestinal tract (*37*). Skill tasks for endoscopic neurosurgery have not previously been developed. To provide a means of comparing manual and robotic operator performance, we proposed a set here by analyzing the steps of tumor resection. It is our hope that these tests can be further developed to establish performance standards in endoscopic neurosurgery.

Limitations

This paper demonstrates the potential of a bimanual robotic endoscope system for minimally invasive neurosurgery. Although the system incorporates all of the critical features needed for neurosurgery, additional refinements are needed before clinical translation. For example, the current trocar cross section dimensions (10 mm by 12 mm) should be scaled down to match that of a standard neurosurgical trocar, such as the 8.3-mm-diameter MINOP InVent trocar (*17*). This could be easily accomplished by reducing the spacing between robot arms, 8 mm, to 4.5 mm (center to center). Comparing with Fig. 2B, the individual arm workspace would be unchanged, whereas the overall width of the bimanual workspace would be reduced by only 3.5 mm.

In addition, the endoscope camera should be replaced with a high-resolution optical system that enables adjustment of tip viewing angle. This could be accomplished using either steerable optics or by designing the optics to be separate and swappable from the trocar, as is the case with existing endoscopes. If space allows, three-dimensional (3D) endoscopy could also be considered.

Inserted through small incisions, endoscopes are an effective tool for reducing the invasiveness of surgical procedures. Their imaging system moves the surgeon′s eyes to the surgical site, providing a substantial improvement over peering into a deep incision. This paper has focused on developing robotic technology that moves the surgeon′s hands to the endoscope tip, equipping them with the manipulation capabilities of open surgery. This includes the ability to perform bimanual tasks, to change tools intraoperatively, and to remove tissue, all without removing the endoscope trocar from the surgical site. Although neurosurgical applications were the focus of this work, the scalable and modular technology described here could be applied to clinical applications throughout the body, for example, in urology and gynecology.

MATERIALS AND METHODS

Robot arm design

Kinematic design

We compared three arm designs in terms of workspace, operational safety, and complexity/cost (fig. S1, A to C). All designs were concentric tube robots fabricated from superelastic NiTi (*31*). The design of fig. S1A was composed of a pair of tubes (light and dark brown) that were precurved. The precurvatures and relative bending stiffness of the tubes were selected so that the tubes were "balanced" (*30*, *31*). When they were rotated such that the precurvatures oppose each other, the combined tubes were straight (green tube on right). When the tubes were rotated such that the curvatures are in the same direction, as shown on the left, the combined tubes (green) took on their maximum curvature. In this way, by rotating the two tubes individually and with respect to each other, while also translating the tubes together in and out of the trocar, a trumpet-

shaped workspace volume could be swept out. The workspace volume can be described by the radius, r_b, corresponding to the configurations when the tubes were maximally extended from the trocar and the precurvatures were aligned.

The design of fig. S1B was also composed of two tubes, but in this case, only the inner tube was precurved, and the stiffness of the outer tube was selected to dominate (be much stiffer, e.g., 10×) than the stiffness of the inner tube. When the outer tube was retracted, the inner tube took on its precurved shape. As the outer tube was extended over the inner tube, it straightened the portion of the inner tube that it had extended over (fig. S1B). By rotating the inner tube and extending and retracting each tube from the trocar, this design also produced a trumpet-shaped workspace with a maximum radius of r_d.

The design of fig. S1C used three tubes and concatenated the previous two designs with a balanced stiffness tube pair at the base that dominates an inner precurved tube at the tip. Although this design produces a more complex workspace shape, its outer boundary is defined by the distal precurved tube, which produces a trumpet shape with radius r_{bd1}. This follows because the precurvature that can be given to a tube is limited by the maximum bending strain in the tube, $\varepsilon \approx r/\rho$, in which r is tube outer radius and ρ is bending radius of curvature. (This equation holds for an unpatterned tube.) Given a maximum bending strain, a smaller-radius tube can be given a smaller radius of precurvature. This means that, in fig. S1C, $r_{bd1} > r_{bd2} > r_{bd3}$.

To compare the three designs, we equated the lumen diameter of the innermost tube in each design because all designs must be able to pass tools of the same diameter. We also equated the maximum tube extension for each design. Imposing these constraints, we observed that $r_d = r_{bd1} > r_b$. The inequality arises because the outer tube of the balanced stiffness design cannot be precurved as much as the inner tube and so increases the combined curvature as shown in fig. S1A (left). The designs of fig. S1 (B and C) have the same diameter workspace. Although the three-tube design of fig. S1C provides some level of tip orientation control, this exceeds the clinical requirement of three–degree of freedom tip positioning. Consequently, we discarded the three-tube design from further consideration.

We first investigated the dominating stiffness design of fig. S1B given its larger workspace and its simpler construction; it uses only a single precurved tube, and careful balancing of tube stiffnesses is not required. When we implemented this design, however, we noted that when the robot arm moved near or through the straight configuration (corresponding to a kinematic singularity), the outer tube translated in and out over the inner tube at high velocity. We became concerned that the distal edge of the outer tube could abrade or tear any tissue touching the side of the arm as the tube moved in and out (a sawing motion). The balanced stiffness tube pair also has a kinematic singularity at the straight configuration, but tube motion here consists, at most, of rapid tube rotations. These motions do not damage tissue contacting the outer tube. Consequently, we abandoned the dominating stiffness design and selected balanced stiffness tube pairs for our robot arm designs.

Tube patterning to maximize arm curvature

In our prior work fabricating balanced stiffness pairs of precurved tubes, we were limited to about 1% maximum bending strain in the outer tube because that is the limit of linear elastic behavior for superelastic NiTi (*32*). (Note that strains for a tube pair as stated here are computed here on the basis of the outer diameter of the outer tube.) When precurving individual tubes, we were able to produce maximum precurvatures of 3 to 4% (*40*), with higher values causing the tubes to buckle. To maximize the radius, r_b, of the workspace, we sought to find a method by which we could overcome both these limits.

To achieve this, we investigated a widely used technique in the manufacture of catheters: the use of lasers to cut patterns of holes in tubing. Such laser-patterned tubing can flex without buckling along tortuous curvatures through the vasculature. Furthermore, on the basis of the pattern design, the bending stiffness of the tube can be tuned. Whereas patterning had previously been considered for enhancing the elastic stability of concentric tube robots (*41*, *42*), we introduce the technique here for two purposes: to enable precurvatures without buckling above 4% strain and to provide a means to balance the stiffness of tube pairs at these strain levels.

Using a diamond-shaped hole pattern (fig. S1D) as motivated by (*42*), we investigated a range of pattern parameters to empirically arrive at the tube designs of table S1. We shape-set these tubes at precurvatures corresponding to 4% strain for the outer tube and 4.5% strain for the inner tube. Shape setting consisted of inserting the tubes into grooves in a template (fig. S1E), placing them in an oven at 520°C for 50 min and then immediately quenching them in cold water. The resulting tube pair, shown in fig. S1F, has a workspace radius of r_b = 17.5 mm, which corresponds to a maximum bending strain in the outer tube of 4.5%. (The inner tube causes it to curve more when the curvatures are aligned.) This produces a workspace diameter for one arm of 35 mm compared with 8.7 mm if patterning had not been used. At full extension, the two arms together have a workspace diameter that is 3.6 times the diameter of the trocar.

To reduce materials cost and maximize torsional arm stiffness, the NiTi robot arms were glued to proximal stainless steel tubes as shown in fig. S1G (*40*). The steel tubes attach at their base to the transmission portion of the arm modules that pass through the trocar and connect the transmission portion of the arm modules as described below and depicted in fig. S2.

Robot arm and tool module design

The details of the arm and tool module mechanisms of Fig. 2 (E and F), are shown in fig. S2. The transmission tubes of the two arms (fig. S1G) connect via collars to individual rotary bearings. Screw gears (fig. S2A) produce tube rotations based on rotation of Hirth couplers (fig. S2B) that mate with matching pairs in the drive system (fig. S2C). In a clinical scenario, a sterile bag incorporating Hirth coupler inserts would be fit between the arm module and the drive system to create a sterile boundary between the sterile arm module and the nonsterile drive system. Flexibility of the stainless-steel transmission tubes and the "snap-in" mating of the Hirth couplers allow the arm modules to be inserted and removed from the trocar module and drive system. Arrays of magnets are used to help align and attach the modules to the mating drive system components, and a pair of screws are used to ensure a strong connection once in place.

The tool modules (fig. S2, D and E) share the same footprint as the arm modules (compare fig. S2B and fig. S2D), and the proximal gear set similarly rotates the tool shaft to produce tool roll. The difference is that the distal gear set drives a hollow screw that translates the tool's pull wire. The pull wire passes through the screw and is

clamped in a nut-mounted bearing. The bearing prevents the pull wire from twisting when the tool rolls.

Owing to a small clearance between the tool shaft and the inner diameter of the arms, the tools slide in and out of the arms easily. To facilitate manual insertion and removal of a robot arm from the trocar, its tubes are first rotated to straighten the arm. In this configuration, the robot arms slide easily in and out of the trocar working channels. When the arms and tools are under robotic control, relative motion among the tools, arms, and trocar was smooth; friction was never observed to be an issue.

As can be seen from fig. S2, the arm and tool modules are compact and composed of inexpensive plastic and metal parts. As a result, the modules can be designed as disposables that can be sterilized at the place of manufacture by steam or ethylene oxide. To demonstrate ease of sterilization, we performed ethylene oxide sterilization of arm and tool modules (fig. S2F).

Robot controller

The robot controller is composed of a 12-V power supply (Mean Well, Taiwan) that drives five two-channel motor drivers (Basicmotion Micro Control, CA). Hall effect sensor switches, connected to an interface board (Phidgets, Canada), were mounted on each linear stage for detecting end of travel conditions. Two six–degree of freedom joysticks (Touch, 3D Systems) with custom tool controllers enabled the users to control the robot arms. The motor controllers, interface board, and joysticks communicated with a PC (Intel Core i7-8550U CPU at 1.80 GHz with 16 GB of RAM) using USB serial connections.

The robot control code, written in C++, receives tip position commands from the two joysticks and converts those to the equivalent rotations and translations of the arm tubes. The code is based on modeling the kinematics using a mechanics-based model (*31*, *43*). If an end-of-travel condition is detected, then the controller pauses the stage at its limit until the user moves back within the range of motion. This provides smooth end-of-workspace motion. The code also implements an emergency stop condition by freezing the motors when an emergency stop button is pressed.

The tool controllers enable the operator to open and close tools such as forceps and scissors on the basis of varying the distance between their middle finger and thumb. A switch located under the forefinger is used to engage and disengage the robot arm and tool. Before engaging the arm, the operator can position the joystick as desired in its workspace and also open and close the fingers to match the current state of the tool.

Fabrication of skill tasks

The boundary separation skill task model (fig. S3A) consists of a white silicone cube representing the brain with a cylindrical hole. The cube was glued to a 3D-printed base to secure it to the black frame (fig. S3D), which was attached to the bottom of the water tank. The cylindrical hole was filled with an olive-shaped silicone capsule representing the tumor. Between the tumor and the brain, an electrically conductive silicone rubber sheet (McMaster-Carr) was attached to detect contact between the tools and the brain while executing the task. Both the brain and the tumor were molded using Dragon Skin silicone (Smooth-On Inc.). The tumor was colored with Silc Pig silicone color pigment (Smooth-On Inc.). Last, four silicone rubber tubes (McMaster-Carr) with outer diameters of 1 mm were passed through the brain using a needle. To mark where the blood vessels are cauterized, the tubes were painted with Dykem Steel Blue Layout Fluid. This paint was selected because it scrapes off when a tool is rubbed over the tubing.

The components of the capsule cutting skill task (fig. S3B) consist of a 3D-printed frame with a stainless-steel weight glued to the bottom of it, a membrane cut out of nitrile exam gloves, and six elastic bands to suspend the membrane from the walls of the water tank. The membrane has a 2-cm-diameter circle stamped in ink to indicate the path that the operator must follow while cutting.

The same Dragon Skin silicone brain and flesh silicone tumor used in the boundary separation task were adopted to build the fibrous debulking test setup (fig. S3C). The fibrotic tumor is composed of seven small cotton pieces spray-painted red to enhance their visibility and mounted on a surgical suture, inside the tumor capsule, using a needle. After removing the needle, the suture is secured around the 3D-printed base, which is then mounted on the black frame (fig. S3D) at the bottom of the water tank.

The hidden ring transfer (fig. S3D) is made from a 3D-printed circular well with eight stainless steel pins mounted on the base. Rings that fit over the pins were constructed from an inner metal core cut from stainless steel tubing that is glued inside a Dragon Skin silicone triangle (side, 6 mm) colored with Silc Pig pigment. After the rings were placed around the corresponding pin, an opaque membrane (cut from a surgical glove) was mounted on top of the well via a lid secured with four screws. The 6-mm hole at the center of the membrane is made with a hole punch. For testing, the well was secured to the black frame at the bottom of the water tank.

Human brain phantom and pineal tumor model

Preoperative computed tomography and magnetic resonance imaging studies were obtained from a 4-month-old child with hydrocephalus secondary to a pineal tumor. These data were obtained with permission from the parents, and all images were de-identified and stored on a secure server to maintain patient confidentiality. The images were used to construct the brain phantom of Fig. 7 (D to F) using the method described in (*44*). This method produces phantom brain tissue with comparable mechanical properties to actual brain tissue. The tumor model (Fig. 7D) was sized to reach from the back to the midpoint of the third ventricle. Our surgeons (J.D. and S.S.) investigated a wide range of fruit flesh to find one with the consistency of brain tumors that can be aspirated. Medium ripe bananas were found to reproducibly provide the desired consistency. A cylindrical tube (diameter, 1.5 cm) was used as a punch to create a banana plug, and this plug was inserted into the silicone tumor capsule body. To incorporate a front capsule surface covering the banana, a layer of 0.1-mm-thick PVC film was used. The film thickness was chosen to approximate an actual pineal tumor capsule that can be torn open using forceps.

Statistical analysis

MATLAB (version R2021b) statistical subroutines were used to analyze the data and perform all statistical tests. Trials were considered outliers in cases of equipment malfunction or if data were less than $Q1 - 1.5 \times IQR$ (interquartile range) or greater than $Q3 + 1.5 \times IQR$, where the $IQR = Q3 - Q1$. Groups, corresponding to different manual and robotic instruments, have unequal sample sizes and

sample variances. We used Levene's test to evaluate equality of variances. With no evidence of normally distributed time duration and different sample size, we used the Mann Whitney *U* nonparametric test to check whether there are statistically significant time differences among two groups (in particular, manual and robotic) for each skill task. Statistical significance was tested at the 5% confidence level ($P < 0.05$).

Supplementary Materials

This PDF file includes:
Figs. S1 to S3
Table S1
Supplementary Data

Other Supplementary Material for this manuscript includes the following:
Movies S1 to S10
MDAR Reproducibility Checklist

REFERENCES AND NOTES

1. National Neurosurgical Procedural Statistics, 2006 Survey, in *National Neurosurgical Procedural Statistics, 2006 Survey* (AANS Rolling Meadows, 2008).
2. M. Ammirati, N. Vick, Y. Liao, I. Ciric, M. Mikhael, Effect of the extent of surgical resection on survival and quality of life in patients with supratentorial glioblastomas and anaplastic astrocytomas. *Neurosurgery* **21**, 201–206 (1987).
3. J. S. Smith, E. F. Chang, K. R. Lamborn, S. M. Chang, M. D. Prados, S. Cha, T. Tihan, S. VandenBerg, M. W. McDermott, M. S. Berger, Role of extent of resection in the long-term outcome of low-grade hemispheric gliomas. *J. Clin. Oncol.* **26**, 1338–1345 (2008).
4. D.-Y. Cho, C.-C. Chen, C.-S. Chang, W.-Y. Lee, M. Tso, Endoscopic surgery for spontaneous basal ganglia hemorrhage: Comparing endoscopic surgery, stereotactic aspiration, and craniotomy in noncomatose patients. *Surg. Neurol.* **65**, 547–555 (2006).
5. J. Abdullah, J. Caemaert, Endoscopic management of craniopharyngiomas: A review of 3 cases. *Sort* **38**, 79–84 (1995).
6. D. Hellwig, B. L. Bauer, M. Schulte, S. Gatscher, T. Riegel, H. Bertalanffy, Neuroendoscopic treatment for colloid cysts of the third ventricle: The experience of a decade. *Neurosurgery* **52**, 525–533 (2003).
7. K. Margetis, M. M. Souweidane, Endoscopic treatment of intraventricular cystic tumors. *World Neurosurg.* **79**, S19.e1–S19.e11 (2013).
8. M. J. Torrens, Endoscopic neurosurgery. *Neurosurg. Q.* **5**, 18–33 (1995).
9. R. P. Naftel, C. N. Shannon, G. T. Reed, R. Martin, J. P. Blount, R. S. Tubbs, J. C. Wellons, Small-ventricle neuroendoscopy for pediatric brain tumor management. *J. Neurosurg. Pediatr.* **7**, 104–110 (2011).
10. E. M. Horn, R. F. Spetzler, Treatment options for third ventricular colloid cysts. *Neurosurgery* **62**, E1384 (2008).
11. T. Fukushima, Endoscopic biopsy of intraventricular tumors with the use of a ventriculofiberscope. *Neurosurgery* **2**, 110–113 (1978).
12. M. M. Souweidane, Endoscopic surgery for intraventricular brain tumors in patients without hydrocephalus. *Neurosurgery* **57**, 312–318 (2005).
13. M. M. Souweidane, N. Luther, Endoscopic resection of solid intraventricular brain tumors. *J. Neurosurg.* **105**, 271–278 (2006).
14. M. R. Gaab, H. W. Schroeder, Neuroendoscopic approach to intraventricular lesions. *J. Neurosurg.* **88**, 496–505 (1998).
15. P. Cappabianca, G. Cinalli, M. Gangemi, A. Brunori, L. M. Cavallo, E. de Divitiis, P. Decq, A. Delitala, F. di Rocco, J. Frazee, U. Godano, A. Grotenhuis, P. Longatti, C. Mascari, T. Nishihara, S. Oi, H. Rekate, H. W. S. Schroeder, M. M. Souweidane, P. Spennato, G. Tamburrini, C. Teo, B. Warf, S. T. Zymberg, Application of neuroendoscopy to intraventricular lesions. *Neurosurgery* **62**, 10.1227/01.neu.0000316262.74843.dd, (2008).
16. C. Teo, P. Nakaji, Neuro-oncologic applications of endoscopy. *Neurosurg. Clin. N. Am.* **15**, 89–103 (2004).
17. BBraun Sharing Expertise, Aesculap MINOP InVent Advanced Intraventricular Neuroendoscopy.
18. G. R. Sutherland, S. Lama, L. S. Gan, S. Wolfsberger, K. Zareinia, Merging machines with microsurgery: Clinical experience with neuroArm. *J. Neurosurg.* **118**, 521–529 (2013).
19. K. Nishizawa, M. G. Fujie, K. Hongo, T. Dohi, H. Iseki, Development of surgical manipulator system "HUMAN" for clinical neurosurgery. *JMAJ* **49**, 335 (2006).
20. H. Takasuna, T. Goto, Y. Kakizawa, T. Miyahara, J. Koyama, Y. Tanaka, T. Kawai, K. Hongo, Use of a micromanipulator system (NeuRobot) in endoscopic neurosurgery. *J. Clin. Neurosci.* **19**, 1553–1557 (2012).
21. E. J. Butler, R. Hammond-Oakley, S. Chawarski, A. H. Gosline, P. Codd, T. Anor, J. R. Madsen, P. E. Dupont, J. Lock, Robotic neuro-endoscope with concentric tube augmentation, in *2012 IEEE/RSJ International Conference on Intelligent Robots and Systems* (IEEE, 2012), pp. 2941–2946.
22. Y. Gao, K. Takagi, T. Kato, N. Shono, N. Hata, Continuum robot with follow-the-leader motion for endoscopic third ventriculostomy and tumor biopsy. *IEEE Trans. Biomed. Eng.* **67**, 379–390 (2020).
23. T. L. H. Azimian, J. Drake, A dual-arm robotic neuroendoscope: Early results, paper presented at the The Hamlyn Symposium on Medical Robotics, London, 2016.
24. M. F. Rox, D. S. Ropella, R. J. Hendrick, E. Blum, R. P. Naftel, H. C. Bow, S. D. Herrell, K. D. Weaver, L. B. Chambless, R. J. Webster, Mechatronic design of a two-arm concentric tube robot system for rigid neuroendoscopy. *IEEE/ASME Trans. Mechatron.* **25**, 1432–1443 (2020).
25. J. Wang, X. Yang, P. Li, S. Song, L. Liu, M. Q. H. Meng, Design of a multi-arm concentric-tube robot system for transnasal surgery. *Med. Biol. Eng. Comput.* **58**, 497–508 (2020).
26. T. L. Bruns, A. A. Remirez, M. A. Emerson, R. A. Lathrop, A. W. Mahoney, H. B. Gilbert, C. L. Liu, P. T. Russell, R. F. Labadie, K. D. Weaver, R. J. Webster III, A modular, multi-arm concentric tube robot system with application to transnasal surgery for orbital tumors. *Int. J. Robot. Res.* **40**, 521–533 (2021).
27. T. Cooper, C. R. Ramstad, Sterile drape interface for robotic surgical instrument (Google Patents, 2011).
28. P. E. Dupont, N. Simaan, H. Choset, C. Rucker, Continuum robots for medical interventions. *Proc. IEEE* **110**, 847–870 (2022).
29. P. E. Dupont, B. J. Nelson, M. Goldfarb, B. Hannaford, A. Menciassi, M. K. O'Malley, N. Simaan, P. Valdastri, G. Z. Yang, A decade retrospective of medical robotics research from 2010 to 2020. *Robotics* **6**, eabi8017 (2021).
30. P. Sears, P. Dupont, A steerable needle technology using curved concentric tubes, *in 2006 IEEE/RSJ International Conference On Intelligent Robots and Systems* (IEEE, 2006), pp. 2850–2856.
31. P. E. Dupont, J. Lock, B. Itkowitz, E. Butler, Design and control of concentric-tube robots. *IEEE Trans. Rob.* **26**, 209–225 (2010).
32. G. Fagogenis, M. Mencattelli, Z. Machaidze, B. Rosa, K. Price, F. Wu, V. Weixler, M. Saeed, J. E. Mayer, P. E. Dupont, Autonomous robotic intracardiac catheter navigation using haptic vision. *Sci. Robot.* **4**, eaaw1977 (2019).
33. J. H. Peters, G. M. Fried, L. L. Swanstrom, N. J. Soper, L. F. Sillin, B. Schirmer, K. Hoffman, the SAGES FLS Committee, Development and validation of a comprehensive program of education and assessment of the basic fundamentals of laparoscopic surgery. *Surgery* **135**, 21–27 (2004).
34. M. Vassiliou, G. A. Ghitulescu, L. S. Feldman, D. Stanbridge, K. Leffondré, H. H. Sigman, G. M. Fried, The MISTELS program to measure technical skill in laparoscopic surgery. *Surg. Endosc. Other Interv. Tech.* **20**, 744–747 (2006).
35. R. Smith, V. Patel, R. Satava, Fundamentals of robotic surgery: A course of basic robotic surgery skills based upon a 14-society consensus template of outcomes measures and curriculum development. *Int. J. Med. Robot. Comput. Assist. Surg.* **10**, 379–384 (2014).
36. G. Sroka, L. S. Feldman, M. C. Vassiliou, P. A. Kaneva, R. Fayez, G. M. Fried, Fundamentals of laparoscopic surgery simulator training to proficiency improves laparoscopic performance in the operating room—A randomized controlled trial. *A. J. Surg.* **199**, 115–120 (2010).
37. M. C. Vassiliou, B. J. Dunkin, G. M. Fried, J. D. Mellinger, T. Trus, P. Kaneva, C. Lyons, J. R. Korndorffer Jr., M. Ujiki, V. Velanovich, M. L. Kochman, S. Tsuda, J. Martinez, D. J. Scott, G. Korus, A. Park, J. M. Marks, Fundamentals of endoscopic surgery: Creation and validation of the hands-on test. *Surg. Endosc.* **28**, 704–711 (2014).
38. V. Chandra, D. Nehra, R. Parent, R. Woo, R. Reyes, T. Hernandez-Boussard, S. Dutta, A comparison of laparoscopic and robotic assisted suturing performance by experts and novices. *Surgery* **147**, 830–839 (2010).
39. A. Zihni, W. D. Gerull, J. A. Cavallo, T. Ge, S. Ray, J. Chiu, L. M. Brunt, M. M. Awad, Comparison of precision and speed in laparoscopic and robot-assisted surgical task performance. *J. Surg. Res.* **223**, 29–33 (2018).
40. A. H. Gosline, N. V. Vasilyev, E. J. Butler, C. Folk, A. Cohen, R. Chen, N. Lang, P. J. del Nido, P. E. Dupont, Percutaneous intracardiac beating-heart surgery using metal MEMS tissue approximation tools. *Int. J. Robot. Res.* **31**, 1081–1093 (2012).
41. D.-Y. Lee, J. Kim, J. S. Kim, C. Baek, G. Noh, D. N. Kim, K. Kim, S. Kang, K. J. Cho, Anisotropic patterning to reduce instability of concentric-tube robots. *IEEE Trans. Robot.* **31**, 1311–1323 (2015).
42. K. A. X. J. Luo, T. Looi, S. Sabetian, J. Drake, Designing concentric tube manipulators for stability using topology optimization, *in 2018 IEEE/RSJ International Conference on Intelligent Robots and Systems (IROS)* (IEEE, 2018), pp. 1764–1769.

43. D. C. Rucker, R. J. Webster III, G. S. Chirikjian, N. J. Cowan, Equilibrium conformations of concentric-tube continuum robots. *Int. J. Robot. Res.* **29**, 1263–1280 (2010).
44. G. E. Breimer, V. Bodani, T. Looi, J. M. Drake, Design and evaluation of a new synthetic brain simulator for endoscopic third ventriculostomy. *J. Neurosurg. Pediatr.* **15**, 82–88 (2015).

Acknowledgments
Funding: This work was supported by NIH R01NS099207 (P.E.D.). **Author contributions:** Conceptualization: J.D. and P.E.D. Methodology: K.P., J.P., M.M., Y.C., D.P., T.L., S.S., J.D., and P.E.D. Investigation: K.P., J.P., M.M., Y.C., S.S., J.D., and P.E.D. Visualization: M.M. and P.E.D. Funding acquisition: P.E.D. Supervision: P.E.D. Writing: K.P., M.M., S.S., J.D., and P.E.D. **Competing interests:** K.P. and P.E.D. are coinventors on a patent application related to the robot technology. **Data and materials availability:** All data needed to evaluate the conclusions in the paper are present in the main text or the Supplementary Materials.

Submitted 9 January 2023
Accepted 29 August 2023
Published 20 September 2023
10.1126/scirobotics.adg6042

Science Robotics

Using robotics to move a neurosurgeon's hands to the tip of their endoscope

Karl Price, Joseph Peine, Margherita Mencattelli, Yash Chitalia, David Pu, Thomas Looi, Scellig Stone, James Drake, and Pierre E. Dupont

Sci. Robot. **8** (82), eadg6042. DOI: 10.1126/scirobotics.adg6042

Science Robotics (ISSN 2470-9476) is published by the American Association for the Advancement of Science. 1200 New York Avenue NW, Washington, DC 20005. The title *Science Robotics* is a registered trademark of AAAS.